

Effect of extracellular volume on the energy stored in transmembrane concentration gradientsReinoud Maex ^{*}*Biocomputation Research Group, University of Hertfordshire, Hatfield AL10 9AB, United Kingdom* (Received 1 July 2019; revised 25 August 2021; accepted 30 September 2021; published 15 October 2021)

The amount of energy that can be retrieved from a concentration gradient across a membrane separating two compartments depends on the relative size of the compartments. Having a larger low-concentration compartment is in general beneficial. It is shown here analytically that the retrieved energy further increases when the high-concentration compartment shrinks during the mixing process, and a general formula is derived for the energy when the ratio of transported solvent to solute varies. These calculations are then applied to the interstitial compartment of the brain, which is rich in Na^+ and Cl^- ions and poor in K^+ . The reported shrinkage of this compartment, and swelling of the neurons, during oxygen deprivation is shown to enhance the energy recovered from NaCl entering the neurons. The slight loss of energy on the part of K^+ can be compensated for by the uptake of K^+ ions by glial cells. In conclusion, the present study proposes that the reported fluctuations in the size of the interstitial compartment of the brain (expansion during sleep and contraction during oxygen deprivation) optimize the amount of energy that neurons can store in, and retrieve from, their ionic concentration gradients.

DOI: [10.1103/PhysRevE.104.044409](https://doi.org/10.1103/PhysRevE.104.044409)**I. INTRODUCTION**

Concentration gradients can be used to store energy [1]. This phenomenon is well known in biology [2–4], and in particular in neuroscience [5], where neurons use ion gradients to generate currents that charge or discharge the capacitive element of their cell membrane, in this manner continually adapting their electrical potential.

Neurons spend 50–60% of the oxygen they consume maintaining an outward gradient for K^+ and inward gradients for Na^+ and Cl^- (for the physiological concentrations of these ions, see Table I) [6–10]. The major part of this oxygen is used by the Na^+/K^+ pump, which is located in the cell membrane separating the intra- and extracellular compartments (the latter compartment being interchangeably called interstitial space in the present text) [7]. The Na^+/K^+ pump hydrolyzes the metabolic intermediary adenosine triphosphate (ATP) to provide the energy for the expulsion of 3 Na^+ ions against the entry of 2 K^+ ions [11,12].

Neurons subsequently use the energy stored in their Na^+ and K^+ gradients for several purposes, such as the secondary transport of other ions [13], the uptake of nutrients such as glucose [2], the re-uptake of released neurotransmitters such as glutamate [14], or, as mentioned above, for the maintenance of an electrical membrane potential of about -65 mV and the exchange of signals with other neurons [9,15].

Failure to provide the necessary energy leads to a breakdown of the ion gradients on a time scale of seconds to minutes [10,16,17]. Because all membrane transport is in principle reversible, including the production of ATP by a backward-running Na^+/K^+ pump [2–4,11,18,19], most of the energy stored in the gradients could be retrieved as work done

by the ions when they mix between the intra- and extracellular compartments.

Apart from having different ion concentrations, the intra- and extracellular compartments of the grey matter of the brain also have strikingly different volumes. Diffusion studies demonstrated that α , the fraction of volume occupied by the interstitial compartment, decreases from 0.4 after birth to 0.2 in adult animals [20–22]. Remarkably, acute energy deprivation and the resulting breakdown of the ion gradients are invariably associated with a shrinkage of the interstitial compartment [23–25]. The opposite movement, expansion of interstitial space by up to 60%, was observed during sleep [26], and is associated with a restoration of the ion gradients [27]. The expansion of interstitial space during sleep has been proposed to enhance the clearance of metabolites by promoting their convective flow [26].

The present theoretical study investigates whether the observed expansion and contraction of extracellular space may serve another purpose, namely, to enhance the quantity of energy that can be stored in, and retrieved from, the ion gradients. Previous studies of the energy balance of neurons, on the contrary, focussed entirely on the homeostasis of the intracellular ion concentrations, and considered extracellular space as an infinite reservoir of constant ionic composition [9,13,28–30].

The text is organized as follows. In Sec. II a two-compartmental model is presented. Section III A introduces various mixing strategies, corresponding to different degrees of cotransport of solvent and solute, and hence to different extents of concomitant volume contraction or expansion. Sections III B–III D analytically derive the work that can be done by mixing of a single compound at constant volume (Sec. III B), or by mixing at changing volume but with the compound's concentration held constant in one compartment (Sec. III C), or by mixing with both volume and concentration

^{*}r.maex1@herts.ac.uk

varying (Sec. III D). The brief Sec. III E explains how the model can be made more flexible by allowing the compound to be buffered in one of the compartments. Two physiological applications are presented in Secs. IV and V. Section IV calculates the work done by multiple ion gradients that simultaneously evolve to their Donnan equilibrium, whereas Sec. V explores the combined contributions of mixing, volume contraction and buffering to the concentration changes that have been observed during acute energy deprivation or ischemia. The Discussion (Sec. VI) focuses on the physiological relevance of the present study. Detailed analytical derivations are referred to the Appendixes.

II. MODEL AND NOTATION

The model consists of two compartments, characterized by their volume V_1 versus V_2 (in units of m^3) and by the concentration (or ionic activity) of a single compound K , K_1 versus K_2 (in units of mol/m^3 or mM). To quantify the stored energy, the maximum amount of work is calculated that can be done when the concentrations and volumes evolve from their initial values K_1^* , K_2^* , V_1^* , and V_2^* to their final values K_1° , K_2° , V_1° , and V_2° . During mixing, the total volume V and the total amount of solute K_{tot} (in units of moles) are conserved:

$$V = V_1^* + V_2^* = \alpha V + (1 - \alpha)V = V_1^\circ + V_2^\circ, \quad (1)$$

and

$$\begin{aligned} K_{\text{tot}} &= V_1^* K_1^* + V_2^* K_2^* = [\alpha K_1 + (1 - \alpha)K_2]V \\ &= V_1^\circ K_1^\circ + V_2^\circ K_2^\circ, \end{aligned} \quad (2)$$

where α denotes the fraction of total volume V occupied by the first compartment. In the derivations and graphs, α will often be used as the independent (dimensionless) variable representing volume (using $V_1^* = \alpha V$). To conform to its meaning in the experimental literature [20–22], α then denotes the fraction of volume taken by interstitial space. Hence at the physiological value of $\alpha = 0.2$, the ratio of interstitial (extracellular) to intracellular volume is 0.2 to 0.8. In addition, if the relative size of the compartments changes during the mixing process, then the final volume V_1° is denoted by ωV , but often

it is more useful to express V_1° as the fractional change w of the initial volume V_1^* , such that $V_1^\circ = wV_1^* = w\alpha V$.

The two compartments are separated by a semipermeable membrane barrier. An element of solute transferred from the second to the first compartment is denoted by

$$dK = d(V_1 K_1) = -d(V_2 K_2).$$

Two special cases will be considered, in which either the volume V_1 (Sec. III B) or the concentration K_1 (Sec. III C) is held constant during the mixing process, so that dK reduces to $V_1 dK_1$ or $K_1 dV_1$, respectively. Section III D then investigates the general case, in which volume and concentration evolve according to a parameter a which quantifies the degree of cotransport of solvent and solute across the membrane,

$$dV = adK, \quad (3)$$

where $dV = dV_1 = -dV_2$, such that parameter a has a positive value when the solvent and solute are transported in the same direction.

Further, for the analytical calculations of energy in Sec. III, only one compound K at a time is considered, and the total energy is assumed to be the sum over all compounds (for applications involving multiple gradients, see Secs. IV and V). All transport is also assumed to be electroneutral. Even if the actual transport mechanism has an electrogenic component, such as with the $3\text{Na}^+/2\text{K}^+$ pump, energy should be considered a function of state that is independent of the path traversed to reach that state [31,32]. Because the intra- and extracellular bulk solutions are electroneutral, apart from the narrow Debye-layer lining the cell membrane [28,33,34], it is always possible to imagine an electroneutral transport strategy to achieve the concentration gradients (see Sec. IV B). In accord with this, the energy stored in the transmembrane electrical potential will be shown to be only a small fraction (<0.01%) of that stored in the ion gradients (Sec. IV C).

With the above conventions, the maximum work done, or Gibbs free energy retrieved, by the passive transport of solute

TABLE I. Intra- and extraneuronal ion concentrations and calculated Donnan equilibria.

Ion species ^d	Physiological ^a concentration (mM)		Donnan equilibrium ^b at $\alpha = 0.2$ (mM)		Transported charges ^c (mM)
	inside	outside	inside	outside	
Na^+	12	143	42.9	19.6	24.7
K^+	140	4	126.5	57.8	-10.8
Cl^-	8	116	23.9	52.3	-12.7
HCO_3^-	10	31	11.5	25.1	-1.2
A^{-e}	134		134		
Total	304	294	338.8	154.8	0

^aBased on Fig. 3 of Ref. [15]

^bAs calculated in Sec. IV.

^cPositive for positive charges entering the cells during mixing.

^dDi-valent ions such as Ca^{2+} have concentrations that are an order of magnitude smaller than those of monovalent ions so that they can, to a first approximation, be neglected in a study of energy storage.

^eImpermeant anions, mostly negatively charged metabolites and macromolecules.

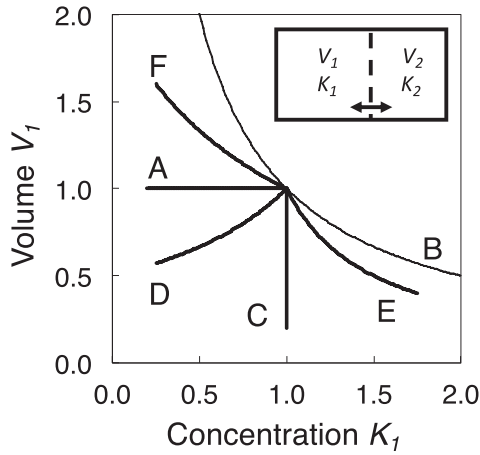


FIG. 1. Diagram of paths plotting volume V_1 of the high-concentration compartment against solute concentration K_1 , both in arbitrary units, starting from an initial state (1, 1). Different paths represent different values of parameter a in Eq. (3), hence different ratios of solvent to solute transport. The paths and their construction are described in greater detail in Sec. III D.

K , can be expressed as

$$W = \Delta G = - \int_{K_1^*}^{K_1^\circ} RT \ln \frac{K_1}{K_2} dK = \int_{K_1^\circ}^{K_1^*} RT \ln \frac{K_1}{K_2} d(K_1 V_1), \quad (4)$$

where R denotes the gas constant ($8.3145 \text{ J mol}^{-1} \text{ K}^{-1}$) and T is the physiological temperature (310 K). Hence the integration over elementary amounts of solute dK leaving the high-concentration compartment, each element multiplied by the current level of the chemical potential (the integrand), generates units of energy.

III. CALCULATION OF THE WORK DONE BY MIXING OF SOLUTE

The present calculations investigate how the work done by mixing of a single compound, flowing down its concentration gradient across a semipermeable membrane barrier [Eq. (4)], depends on the volume ratio of the compartments [parameter α in Eq. (1)], and on the cotransport of solvent, hence on volume changes occurring during the mixing process [parameter a in Eq. (3)].

A. Mixing strategies

Different mixing strategies, corresponding to different ratios of solvent to solute transport [different values of parameter a in Eq. (3)], are represented by different paths on the volume-concentration diagram of Fig. 1. Each path plots the evolution of the volume V_1 and solute concentration K_1 of the high-concentration compartment during the mixing process, using arbitrary units. The complementary paths for the low-concentration compartment (not shown) are completely determined from the conservation of total volume [Eq. (1)] and the conservation of the number of solute particles [Eq. (2)]. A detailed description of this diagram is deferred to Sec. III D, but here the main mixing strategies are introduced.

Path A represents classical mixing at constant volume. There is no cotransport of solvent, and any changes in concentration are exclusively caused by the transmembrane flow of solute (for instance through the Na^+/K^+ pump). This strategy is dealt with in Sec. III B.

Path B plots the other extreme, in which only the solvent is transported. Since there is no solute transport, no work is done by mixing [Eq. (4)], and this path is drawn for reference only.

A disadvantage of strategy A is that the concentration gradient rapidly declines during the mixing process. In strategy C, in contrast, concentration K_1 is held constant by a concomitant contraction of the high-concentration compartment, whose volume V_1 decreases. In this special case of the cotransport of solvent and solute, the solute flows to the low-concentration compartment at a concentration identical to that of the high-concentration compartment it leaves (for instance via ion-water cotransporter channels).

Strategy C will be shown to be superior to A (Sec. III C) but may still not be optimal because, after mixing, a residue of high-concentration solute is left within the contracted compartment (provided its final volume is finite). This residue could have been used to do work during the mixing process. Section III D therefore investigates other ratios of solvent to solute transport. Three of these are represented by paths D–F in Fig. 1; their construction is explained by Eq. (23) in Sec. III D.

B. Mixing with fixed barrier between the compartments

The first special case arises when the volume of the two compartments is held constant, hence $V_1 = V_1^\circ = V_1^*$ and $V_2 = V_2^\circ = V_2^*$ (see path A in Fig. 1). Equation (4) then reduces to

$$\frac{\Delta G}{RT} = V_1^* \int_{K_1^\circ}^{K_1^*} \ln \frac{K_1}{K_2} dK_1. \quad (5)$$

Solving this integral [Appendix A, Eq. (A1)] yields the classical formula for the work of mixing at constant volume [31]:

$$\frac{\Delta G}{RT} = V_1^* (K_1^* \ln K_1^* - K_1^\circ \ln K_1^\circ) + V_2^* (K_2^* \ln K_2^* - K_2^\circ \ln K_2^\circ), \quad (6)$$

or, using Eq. (1),

$$\begin{aligned} \frac{\Delta G}{RTV} &= \alpha (K_1^* \ln K_1^* - K_1^\circ \ln K_1^\circ) + (1 - \alpha) \\ &\quad \times (K_2^* \ln K_2^* - K_2^\circ \ln K_2^\circ). \end{aligned} \quad (7)$$

If the mixing continues until the compound K is fully equilibrated at its final concentration $K_e = K_1^\circ = K_2^\circ$, with

$$K_e = \frac{K_{\text{tot}}}{V} = \frac{V_1^* K_1^* + V_2^* K_2^*}{V} = \alpha K_1^* + (1 - \alpha) K_2^*, \quad (8)$$

then the mixing is complete and Eq. (7) can be rewritten as

$$\begin{aligned} \frac{\Delta G}{RTV} &= \alpha K_1^* \ln K_1^* + (1 - \alpha) K_2^* \ln K_2^* \\ &\quad - [\alpha K_1^* + (1 - \alpha) K_2^*] \ln [\alpha K_1^* + (1 - \alpha) K_2^*]. \end{aligned} \quad (9)$$

The blue curve in Fig. 2, labeled $V_1 \text{const}$, plots the work done by complete mixing of the intra- and extracellular

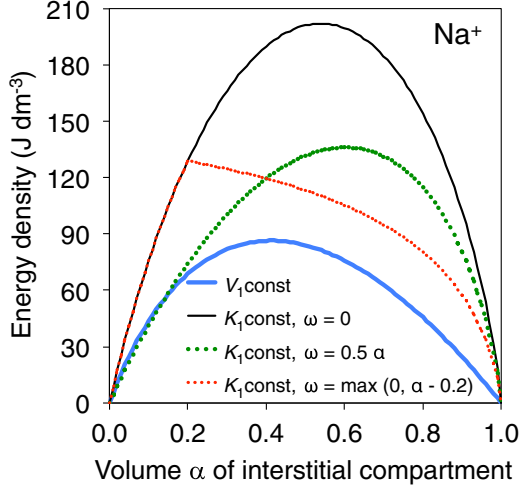


FIG. 2. Energy density in joules per liter retrieved from the physiological concentration gradient of Na^+ (Table I). Work done was calculated for four different mixing strategies during which either the volume of interstitial space (curve labeled V_1, const), or the Na^+ concentration therein (curves labeled K_1, const), was held constant. In the first case (V_1, const) mixing was complete. In the latter cases (K_1, const), the interstitial compartment shrank during mixing from its initial volume fraction α either to zero ($\omega = 0$), or to half its initial volume α ($\omega = 0.5\alpha$), or to a final volume that was less than α by an absolute value of 0.2 [$\omega = \max(0, \alpha - 0.2)$].

Na^+ ions, starting from their physiological concentrations in Table I. The horizontal axis plots the volume fraction α occupied by extracellular space, which is the high-concentration compartment for Na^+ . The work done by mixing at constant volume reaches its peak value of 86 J/l at a volume fraction $\alpha = 0.41$. At this maximum the derivative of Eq. (9) with respect to α ,

$K_1^* \ln K_1^* - K_2^* \ln K_2^* - (K_1^* - K_2^*) \{ \ln[\alpha K_1^* + (1 - \alpha) K_2^*] + 1 \}$, must vanish, hence

$$\begin{aligned} \ln[\alpha K_1^* + (1 - \alpha) K_2^*] &= \frac{K_1^* (\ln K_1^* - 1) - K_2^* (\ln K_2^* - 1)}{(K_1^* - K_2^*)} \\ &= \frac{K_1^* \ln K_1^* - K_2^* \ln K_2^*}{K_1^* - K_2^*} - 1 \end{aligned}$$

or

$$\begin{aligned} \alpha_{\text{opt}} &= \frac{\exp\left(\frac{K_1^* \ln K_1^* - K_2^* \ln K_2^*}{K_1^* - K_2^*} - 1\right) - K_2^*}{K_1^* - K_2^*} \\ &= \frac{K_1^* [K_1^*/(K_1^* - K_2^*)] K_2^* [-K_2^*/(K_1^* - K_2^*)] e^{-1} - K_2^*}{K_1^* - K_2^*}. \end{aligned} \quad (10)$$

As expected from the problem formulation [Eq. (5)], multiplying K_1^* and K_2^* by the same constant does not change the value of α_{opt} in Eq. (10), so that, denoting by K^* the ratio K_1^*/K_2^* ,

$$\alpha_{\text{opt}} = \frac{K^* [K^*/(K^* - 1)] e^{-1} - 1}{K^* - 1}. \quad (11)$$

This function has a value of 0.5 at $K^* = 1$, and approaches $1/e$ or $(1 - 1/e)$ for $K^* \rightarrow \infty$ or $K^* \rightarrow 0$, respectively.

Hence, for optimal energy storage at fixed volume, the high-concentration compartment must take a fraction of the total volume between 0.37 and 0.5, depending on the magnitude of the gradient [35]. The greater the gradient the lesser α_{opt} . Denoting by K_1^* and K_2^* , respectively, the extra- and intracellular concentrations of the monovalent ions of Table I, α_{opt} takes values of 0.412 (Na^+), 0.609 (K^+ , which has an outward directed gradient), 0.408 (Cl^-), and 0.455 (HCO_3^-).

The optimal volume fraction α_{opt} [Eq. (11)] can be understood as follows. For optimal energy retrieval, the compartmental sizes should be such that (1) a maximum amount of high-potential compound is available for downhill transport, while at the same time (2) during transport the concentration gradient is maintained as long as possible. To quantify the amount of high-potential solute, the equilibrium concentration K_e must be subtracted from the initial concentration K_1^* present within the high-concentration compartment. This quantity then measures, using Eq. (8),

$$\begin{aligned} \alpha(K_1^* - K_e) &= \alpha\{K_1^* - [\alpha K_1^* + (1 - \alpha) K_2^*]\} \\ &= \alpha(1 - \alpha)(K_1^* - K_2^*), \end{aligned}$$

and maximizes at $\alpha = 0.5$. On the other hand, maintaining the concentration gradient after an infinitesimal amount of solute ΔK has been transferred requires minimizing (see Appendix A),

$$\lim_{\Delta K \rightarrow 0} \frac{1}{\Delta K} \left(\ln \frac{K_1}{K_2} - \ln \frac{K_1 - \frac{\Delta K}{V_1}}{K_2 + \frac{\Delta K}{V_2}} \right) = \frac{1}{\alpha V K_1} + \frac{1}{(1 - \alpha) V K_2}, \quad (12)$$

the derivative of which with respect to α vanishes at

$$\alpha = \frac{\sqrt{K_1 K_2} - K_2}{K_1 - K_2}. \quad (13)$$

The optimal value of α in Eq. (13) approaches 0.5 and 0.0 for $K_1 \rightarrow K_2$ and $K_1 \rightarrow \infty$, respectively. Hence, using solely Eq. (13) as optimality criterion, interstitial space should take a volume fraction α of 0.225 (using the Na^+ gradient), 0.86 (K^+), 0.208 (Cl^-), or 0.362 (HCO_3^-).

In summary, from the considerations in this subsection, it is clear that for mixing at constant volume (along path A in Fig. 1) the low-concentration compartment should be greater than the high-concentration compartment.

Finally, for large gradients ($K_1^* \gg K_2^*$), the stored energy scales almost linearly with the magnitude of the gradient $K^* = K_1^*/K_2^*$, as the partial derivative of Eq. (9) with respect to K^* approximates the constant

$$\lim_{K^* \rightarrow \infty} \alpha K_2^* \ln \frac{K^* K_2^*}{[\alpha K^* K_2^* + (1 - \alpha)]} = -K_2^* \alpha \ln \alpha.$$

C. Mixing with movable barrier and fixed concentration in the high-concentration compartment

The second special case of Eq. (4) arises when, during mixing, the concentration K_1 in the high-concentration compartment remains clamped at its initial value K_1^* (see path C in Fig. 1). This requires that, when an element of solute $d(K_1 V_1)$ diffuses across the membrane barrier, solvent is extruded as well, and the compartment shrinks. If the compartmental

volume V_1 thereby decreases to zero, then Eq. (4) reduces to

$$\frac{\Delta G}{RT} = K_1^* \int_0^{V_1^*} \ln \frac{K_1^*}{K_2} dV_1. \quad (14)$$

This integral can be solved (Appendix B) to yield

$$\begin{aligned} \frac{\Delta G}{RT} = & V_1^* K_1^* \ln K_1^* + V_2^* K_2^* \ln K_2^* - K_{\text{tot}} \ln \frac{K_{\text{tot}}}{V} \\ & - (K_1^* - K_2^*) V_2^* \ln \frac{V_2^*}{V}, \end{aligned} \quad (15)$$

which can be rewritten, using Eq. (1), as

$$\begin{aligned} \frac{\Delta G}{RTV} = & \alpha K_1^* \ln K_1^* + (1 - \alpha) K_2^* \ln K_2^* - [\alpha K_1^* \\ & + (1 - \alpha) K_2^*] \ln [\alpha K_1^* + (1 - \alpha) K_2^*] \\ & + (K_2^* - K_1^*) (1 - \alpha) \ln(1 - \alpha). \end{aligned} \quad (16)$$

Comparing Eq. (16) with Eq. (9) yields

$$\left(\frac{\Delta G}{RTV} \right)_{K_1} = \left(\frac{\Delta G}{RTV} \right)_{V_1} + (K_2^* - K_1^*) (1 - \alpha) \ln(1 - \alpha), \quad (17)$$

where the subscripts K_1 and V_1 indicate the quantity held constant. Note that, apart from the position of the barrier, the final states are identical in these two mixing strategies ($K^\circ = K_e$ over the entire volume V). Moreover, the supplemental term in Eq. (17) is non-negative because $0 \leq (1 - \alpha) \leq 1$ and $K_1^* > K_2^*$. This term can therefore be thought of as the osmotic work done by the second compartment during the mixing process. Indeed, if the mixing starts from iso-osmotic conditions, then the second (low-concentration) compartment must contain impermeant solute particles, $(K_1^* - K_2^*) (1 - \alpha) V$ moles in total, that balance the concentration difference for K . This supplemental term then represents the isothermal work that can be done by these particles when they diffuse, during expansion of the second compartment, from their initial volume fraction $(1 - \alpha)$ to the entire volume. [Strictly speaking, the assumption $K_1^* > K_2^*$ is not required for the derivation of Eq. (17). The supplemental term is negative when the high-concentration compartment expands instead of shrinking, as will be illustrated in Sec. III D].

In Eq. (16), the work done is maximal at the value α_{opt} at which the derivative with respect to α vanishes. Using again K^* to denote K_1^*/K_2^* , and assuming K_1^* to be the concentration that is held constant during the mixing process,

$$\alpha_{\text{opt}} = 1 - \frac{K^*}{K^*[K^*/(K^*-1)] + K^* - 1}. \quad (18)$$

This function has limits of 0.5 for $K^* \rightarrow \infty$, $(1 - 1/e)$ for $K^* \rightarrow 1.0$, and 1.0 for $K^* \rightarrow 0$. Hence, if the high-concentration compartment shrinks to zero volume at constant concentration K_1 (this implies $K_1^* \geq K_2^*$), then it should take a fraction α_{opt} of the total volume between 0.5 and 0.63, depending on the magnitude of the gradient.

In Fig. 2, the black curve labeled $K_1 \text{ const}$, $\omega = 0$ represents the work done by the mixing of the physiological Na^+ gradient, when the interstitial compartment shrinks from its initial volume fraction α to zero without changing its Na^+ concentration. Compared to complete mixing at constant volume (blue

curve) the retrieved energy more than doubles (peak value of 202 J/l at $\alpha = 0.54$ versus 86 J/l at $\alpha = 0.41$).

The above calculations Eqs. (14)–(18) concerned the hypothetical case in which the high-concentration compartment shrinks to zero volume. If, instead, this compartment shrinks from its initial volume $V_1^* = \alpha V$ to a finite volume $V_1^\circ = \omega V$, then Eq. (14) reads

$$\begin{aligned} \frac{\Delta G}{RT} = & K_1^* \int_{\omega V}^{\alpha V} \ln \frac{K_1^*}{K_2} dV_1 \\ = & K_1^* \int_0^{\alpha V} \ln \frac{K_1^*}{K_2} dV_1 - K_1^* \int_0^{\omega V} \ln \frac{K_1^*}{K_2} dV_1. \end{aligned} \quad (19)$$

The first integral is solved by Eq. (16), the second by the same equation but with the initial value $K_2^{*'} at $V_1 = \omega V$ now given by$

$$K_2^{*' = \frac{K_{\text{tot}} - \omega V K_1^*}{(1 - \omega)V}.$$

Substitution yields immediately

$$\begin{aligned} \frac{\Delta G}{RTV} = & (\alpha - \omega) K_1^* \ln K_1^* + (1 - \alpha) K_2^* \ln K_2^* - (K_{\text{tot}} \\ & - \omega K_1^*) \ln (K_{\text{tot}} - \omega K_1^*) \\ & + (K_2^* - K_1^*) (1 - \alpha) \ln(1 - \alpha) \\ & + K_1^* (1 - \omega) \ln(1 - \omega). \end{aligned} \quad (20)$$

The value of α that maximizes Eq. (20) is then given, using K^* to denote K_1^*/K_2^* , by

$$\alpha_{\text{opt}} = 1 - \frac{K^*(1 - \omega)}{K^*[K^*/(K^*-1)] + K^* - 1}. \quad (21)$$

Volume contractions of 50% and more have been observed for the interstitial compartment of the brain [21,25,26,36]. To estimate the energy that can be gained from contractions of this extent, the work done by mixing of the physiological Na^+ gradient was recalculated using Eq. (20). Two illustrative cases are plotted in Fig. 2. The green-dotted curve (labeled $K_1 \text{ const}$, $\omega = 0.5\alpha$) represents a *relative* contraction of interstitial space by 50% from each initial volume α . Its peak energy measures 136 J/l at $\alpha = 0.6$. In comparison with mixing at constant volume (blue curve), the peak is moved towards greater values of α because when α was increased, the extent of the contraction was greater in absolute terms, and hence more solute would leave the high-concentration compartment, within which the concentration was held constant.

The red-dotted curve [labeled $K_1 \text{ const}$, $\omega = \max(0, \alpha - 0.2)$] therefore illustrates the case in which, during mixing, interstitial space always shrank by 20% of the total volume V , hence the *absolute* volume of contraction was independent of the initial volume α . From the location of the energy peak of 129 J/l at $\alpha = 0.2$, it is clear that if there were, for instance, a mechanical limit on the absolute volume by which the high-concentration compartment could shrink, then no further energy would be gained from assigning this compartment a greater volume than this limit (the reason being that having a greater *low*-concentration compartment now becomes imperative, as explained in Sec. III B). If this 20% limit on the volume of contraction were further reduced, however, to a level below 12% of the total volume V (using the present

sodium gradient), then the (red) energy curve, whose rising leg coincides with the black curve of full contraction, would partially fall below the energy curve of complete mixing at constant volume (blue). The reason for this anomaly is that the interstitial Na^+ concentration is held constant in the present strategy, and hence the mixing may be very incomplete when the shrinkage is only of limited extent. Other mixing strategies, described in the next subsection, can prevent this anomaly.

D. Mixing with both concentration and volume varying

In the general case, which covers the special cases of Secs. III B and III C, an elementary volume dV of solvent is transported in linear proportion a to an element of solute dK , taking again ideal solutions in which only the solvent contributes to the volume. For convenience, Eq. (3) is repeated here:

$$dV = adK, \quad (22)$$

in which the constant a expresses the fixed stoichiometry between solvent and solute transport [13,37]. Provided $a \neq 0$, a^{-1} represents the concentration at which compound K is transported within the element of solvent dV . Depending on the value of a , the following cases can be distinguished, as illustrated by their labeled paths in Fig. 1:

(A) $a = 0$, there is no cotransport of solvent, hence the compartmental volumes remain constant. This case was presented in Sec. III B.

(B) $a \rightarrow \infty$, there is no transport of solute. Any changes in concentration are exclusively caused by shrinkage or expansion of the compartment, hence by transport of solvent.

(C) $aK_1^* = 1$, the concentration at which solute is transported is equal to that within the compartment it leaves. Hence during shrinkage of the compartment, the concentration K_1 remains constant at K_1^* . This case, which can be called iso-osmotic transport, was investigated in Sec. III C.

(D) $0 < aK_1^* < 1$, the transported element of solution is hyperosmotic with respect to the compartment it leaves. Hence the concentration K_1 decreases when the compartment shrinks. The flow of solvent and solute can only continue until no solute is left within a final volume $V_1^\circ > 0$.

(E) $aK_1^* > 1$, the transported element of solution is hypo-osmotic. Hence the concentration K_1 rises when the compartment shrinks, but this rise is less than what would result from a mere volume contraction without solute transport.

(F) $a < 0$, solute and solvent move in opposite directions, or the high-concentration compartment expands while solute flows out of it.

Along the limiting path B ($a \rightarrow \infty$), no work is done by mixing of solute [Eq. (4)]. In the five other strategies, energy can be retrieved from solute leaving the high-concentration compartment, whose volume can be constant (A), decrease (C–E), or increase (F).

Note that the illustrative paths in Fig. 1 were constructed by setting parameter a in Eq. (22) equal to 0 (A), ∞ (B), 1 (C), 0.5 (D), 2 (E), and -1 (F), and that the vertical asymptote of each hyperbolic path is located at $K_1 = a^{-1}$ [see next Eq. (23)].

As explained in Appendix D [Eqs. (D2) and (D6)], provided $aK_1^* \neq 1 \neq aK_2^*$, the following relations are maintained during evolution of the system from its initial to final state:

$$V_1 = \frac{C}{1 - aK_1} \quad \text{and} \quad V_2 = \frac{D}{1 - aK_2}, \quad (23)$$

where the integration constants C and D are determined by the initial conditions

$$C = V_1^*(1 - aK_1^*) \quad \text{and} \quad D = V_2^*(1 - aK_2^*).$$

The amount of work that can be done is then given by [see Eq. (D10)]

$$\begin{aligned} \frac{\Delta G}{RT} = & [V_1 K_1 \ln K_1]_{K_1^\circ}^{K_1^*} + [V_2 K_2 \ln K_2]_{K_2^\circ}^{K_2^*} - \left[\frac{C}{a} \ln V_1 \right]_{V_1^\circ}^{V_1^*} \\ & - \left[\frac{D}{a} \ln V_2 \right]_{V_2^\circ}^{V_2^*}. \end{aligned} \quad (24)$$

This formula is elaborated on in Appendix D, where it is also shown [Eq. (D19)] that the value of parameter a can be derived from the initial (K_1^* and K_2^*) and final concentrations (K_1° and K_2°) and the initial volume $V_1^* = \alpha V$, such that

$$a = \frac{\alpha(K_1^* - K_1^\circ) + (1 - \alpha)(K_2^* - K_2^\circ)}{\alpha(K_1^* - K_1^\circ)K_2^\circ + (1 - \alpha)(K_2^* - K_2^\circ)K_1^\circ}. \quad (25)$$

In addition, the final volume V_1° can be expressed as the fractional change w of V_1^* , such that $V_1^\circ = wV_1^*$, where w is given by [see Eq. (D20)]

$$w = (1 - aK_1^*) / (1 - aK_1^\circ). \quad (26)$$

Equations (24)–(26) will be applied in Sec. V to analyze the changes observed in the brain's interstitial compartment during ischemia.

Alternatively, the value of w may be given, along with α , K_1^* , K_2^* , and K_1° , and in that case the values of a and K_2° are fully determined. This is the protocol adopted in Fig. 3. This figure illustrates the work done by (complete or partial) mixing during contraction (b) or expansion of the high-concentration compartment (d), with the associated values of a^{-1} plotted in (a) and (c).

The sodium gradient (Table I) was chosen in Figs. 3(a) and 3(b) to further demonstrate the effects of volume contraction on the work done by mixing, hence $K_1^* = 143$ mM and $K_2^* = 12$ mM. For all four curves, the size of interstitial space was shrunk by 50% from each initial value α , hence $w = 0.5$, but different mixing strategies were implemented by assigning different values to the final concentration K_1° . The green-dotted curve labeled K_1 const, with peak energy of 136 J/l at $\alpha = 0.6$, can be taken as the point of reference. As in Fig. 2, it represents the work done along path C in Fig. 1, with concentration K_1 held constant in the contracting compartment, hence $K_1^\circ = K_1^*$. The green horizontal line in (a) confirms that Na^+ was transported at a concentration a^{-1} of 143 mM.

As argued in Sec. III A, after such iso-osmotic transport (path C, and by extension also path E in Fig. 1), a high-concentration residue of solute (Na^+) is left within the contracting compartment (interstitial space). Its energy can be assessed by mixing the residual gradient, in a second stage, at

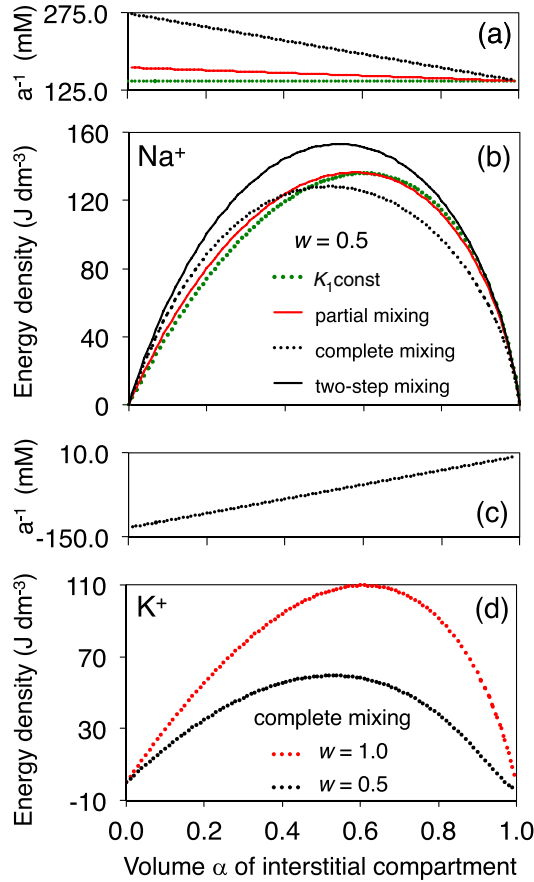


FIG. 3. Work done by mixing strategies with various ratios of solvent to solute transport. The quantity a^{-1} plotted in (a) and (c) represents the concentration at which solute either left (positive values) or entered (negative) interstitial space. Panels (a) and (b) illustrate mixing of the physiological Na^+ gradient of Table I, for (c) and (d) the K^+ gradient was used. Since these gradients have opposite directions, a contraction of interstitial space corresponds to a contraction or expansion, respectively, of the high-concentration compartment of Na^+ or K^+ . During mixing, the volume of interstitial space shrank by 50% ($w = 0.5$) from its initial value α for all curves, except for the curve labeled $w = 1.0$ in (d), which represents mixing at constant volume. After mixing, the concentration K_1° in interstitial space was that of complete mixing K_e [Eq. (8)], except for the curve “ K_1 const” where $K_1^\circ = K_1^*$ and for the curve “partial mixing” where $K_1^\circ = 0.8K_1^* + 0.2K_e$. Mixing in the “two-step” case was accomplished in two stages: first mixing at constant K_1 followed by mixing at constant volume.

constant volume. This is shown in Fig. 3(b) by the black-solid curve labeled two-step mixing, which reaches a higher peak energy of 153 J/l at $\alpha = 0.54$.

A strategy to achieve complete mixing in a single stage is to let the solute leave the contracting high-concentration compartment at a higher concentration than that needed to keep K_1 constant (along path D in Fig. 1). This is illustrated by the black-dotted curve labeled complete mixing for which the final concentration K_1° was imposed to be equal to the equilibrium concentration K_e of Eq. (8). Figure 3(a) shows that the Na^+ ions traveled from interstitial to intracellular space at a concentration a^{-1} (black-dotted line) that was indeed

higher than the (initial) interstitial Na^+ concentration (green). As shown in Fig. 3(b), however, the work this strategy can deliver (black-dotted curve) is less than that of iso-osmotic transport (green), with peak values of 128 J/l at $\alpha = 0.51$, and 136 J/l at $\alpha = 0.6$, respectively. Thus there is a tradeoff between recruiting all solute for transport and keeping the concentration gradient high throughout the mixing process.

Nevertheless, slightly more work can still be done in a single stage if the mixing is only partial, as shown by the red curve in Fig. 3(b), whose peak energy measures 136.5 J/l at $\alpha = 0.58$. Here the final interstitial Na^+ concentration was imposed to be $K_1^\circ = 143 - 0.2 \times (143 - K_e)$, hence K_1 traversed only 20% of the gap between K_1^* and K_e . Accordingly, the Na^+ ions left the interstitial compartment at a concentration a^{-1} [red line in Fig. 3(a)] that was an average of the green and black lines weighted in a ratio of 0.8 to 0.2.

Evidently, the amount of work that can be gained from such partial mixing becomes more substantial when more high-concentration solute would be left, hence when the shrinkage is of lesser extent (not shown). Note also that each of the four cases of mixing with contraction produced a peak energy that was higher than that of mixing at constant volume, the latter strategy, represented by the blue curve in Fig. 2, having a peak energy of 86 J/l at $\alpha = 0.41$.

In contrast, if the high-concentration compartment expands instead of shrinking, along path F instead of path D in Fig. 1, then the work done is less than that of mixing at constant volume (path A). This conclusion was implicit in Eq. (17), and can also be inferred from Eq. (D7) in Appendix D. Figures 3(c) and 3(d) illustrate this result by the work of complete mixing of the K^+ gradient of Table I, hence $K_1^* = 4$ mM, $K_2^* = 140$ mM, and $K_1^\circ = K_e = K_2^\circ$. For the black-dotted curve labeled $w = 0.5$, interstitial space was shrunk again by 50%, leading to a dilation (of varying extent) of potassium’s high-concentration intracellular compartment. Less work was done in this case [black curve in (d)] than by mixing at constant volume (red curve labeled $w = 1.0$), with peak energies of 59 J/l at $\alpha = 0.53$ and 110 J/l at $\alpha = 0.61$, respectively. Figure 3(c) shows, in addition, that the parameter a was negative at all but the highest interstitial volumes α , indicating that solvent and solute moved in opposite directions. Hence water was transported from the interstitial to the cellular compartment, while K^+ flowed in the opposite direction down its concentration gradient. At $\alpha > 0.97$, however, the value of a is positive because the cellular compartment was dilated to such an extent that the concentration K_2 would have fallen below its imposed final value $K_2^\circ = K_e$ [Eq. (8)] if K^+ ions were not transported *up* their gradient (from extra- to intracellular space), at the expense of work and with, as a result, a negative value for the retrieved energy in Fig. 3(d).

E. Mixing with solute buffered in one of the compartments

When the solute moves from one compartment to another, only part of the transported particles may contribute to raising the concentration in the recipient compartment, the other fraction being buffered. Conversely, a buffer located in the donor compartment will lead to a lesser decrease of the concentration therein. Hence, not unlike volume contraction, buffering

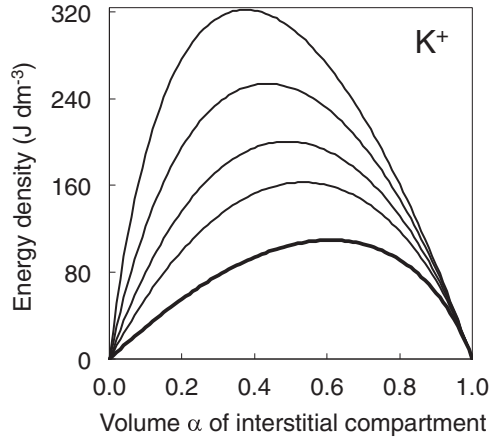


FIG. 4. Effect of the buffering of solute particles on the work done, at constant volume α , by a complete mixing of the K^+ gradient of Table I. The buffer was located in the interstitial compartment. Curves of increasing amplitude represent increasing buffering capacity, corresponding to values of γ in Eq. (27) equal to 0, 1, 2, 4, and 8, or to fractions of 0, 50, 66, 80, or 89% of the K^+ ions being buffered.

is expected to maintain the concentration gradient at a higher level throughout the mixing process.

Without loss of generality, it is assumed here that compound K is buffered in the second compartment, and that its concentration still measures K_2 mM. Equation (2) then extends to

$$K_{\text{tot}} = K_1V_1 + K_2V_2 + \gamma K_2V_2, \quad (27)$$

where the last term indicates the amount of K taken up by the buffer, implying that a fraction

$$\frac{\gamma}{1 + \gamma}$$

of compound K has been buffered within volume V_2 . Rewriting Eq. (27) as

$$K_{\text{tot}} = K_1\alpha V + K_2(1 - \alpha)(1 + \gamma)V$$

makes clear that buffering is equivalent to an extension of the buffering compartment by a volume

$$V_b = (1 - \alpha)\gamma V, \quad (28)$$

so that the extended total volume can be written as

$$V_{\text{ext}} = V_1 + V_2 + V_b = \alpha V + (1 - \alpha)(1 + \gamma)V. \quad (29)$$

To calculate the work of mixing at constant volume, Eq. (6) is still valid provided the extended volumes are substituted. Generalizations of buffering to mixing at nonconstant volume (the strategies described in Secs. III C and III D) are derived in Appendixes C and E.

Figure 4 illustrates the effect of buffering on the work done, at constant volume, by a complete mixing of the K^+ gradient. The buffer was located in interstitial space (the low-concentration compartment of K^+) because the auxiliary glial cells are well known to prevent sharp rises in the interstitial K^+ concentration by taking up K^+ ions released by neurons [25,38,39] (for a detailed argument, see Sec. VI). The buffering capacity was varied in Fig. 4 by incrementing, from 0

(bold curve) to 8, the value of γ in Eq. (27). The graphs show that, in addition to increasing the retrieved energy, buffering also moved the optimal volume α_{opt} in the direction of smaller sizes of the buffering compartment. As already shown by the red curve in Fig. 3(d), the work of unbuffered mixing peaked at $\alpha = 0.61$ (peak value of 110 J/l). With increasing buffering capacity, the optimal volume of interstitial space decreased to values of $\alpha = 0.53$ ($\gamma = 1$; peak value of 163 J/l), 0.49 ($\gamma = 2$; 201 J/l), 0.44 ($\gamma = 4$; 254 J/l), and 0.37 ($\gamma = 8$; 322 J/l).

IV. QUANTIFICATION OF THE ENERGY STORED IN THE PHYSIOLOGICAL ION GRADIENTS IN THE PRESENCE OF IMPERMEANT INTRACELLULAR ANIONS

The membrane-impermeant (and hence immiscible) anions residing within the intracellular compartment (collectively denoted by A^- in Table I) have been neglected so far in the calculations, apart from the suggestion that they may provide the osmotic forces underlying the volume changes in Sec. III C. Nevertheless, their presence prevents the permeant ions from fully equilibrating between the intra- and extracellular compartments. Indeed, a complete mixing of all permeant ions would, in the presence of A^- , violate the electroneutrality of the bulk solutions. The equilibrium concentrations that satisfy electroneutrality constitute the Donnan equilibrium [13,31,33], and must be calculated simultaneously for all ion species involved. Table I lists, for instance, the values of the Donnan equilibrium at an extracellular volume fraction α of 0.2.

In the following, Sec. IV A quantifies the total work done by the permeant ions during their evolution, at constant volume, to the Donnan equilibrium. Sections IV B and IV C verify two related assumptions made in the present study (see Sec. II): first, that the considered ion gradients can be generated in an electroneutral manner by the electrogenic $3Na^+/2K^+$ pump (Sec. IV B), and second, that the energy stored in the electrical membrane potential can be neglected in comparison with that stored in the ion gradients (Sec. IV C).

A. Quantification of the work done by multiple ion gradients mixing to their Donnan equilibrium

Starting from the physiological ion concentrations of Table I, the concentrations at Donnan equilibrium were calculated by solving, for each given interstitial volume α , a set of nine algebraic equations: two for electroneutrality of the intra- and extracellular compartments, four for the conservation of the number of particles of each permeant ion species [Eq. (2)], and three for the coincidence of their Nernst potentials. The physiological concentrations and those at Donnan equilibrium were then substituted into Eq. (7) to calculate the work done by mixing at constant volume. Figure 5 dissects the total work (black curve labeled Donnan) into the work done by each individual ion species. In accordance with the sign and magnitude of each gradient (Sec. III B), the component energies peak at $\alpha = 0.39$ (Na^+ , peak energy of 79 J/l), 0.63 (K^+ , 104 J/l), 0.4 (Cl^- , 68 J/l), and 0.5 (HCO_3^- , 5 J/l), with the total energy peaking at $\alpha = 0.5$ (244 J/l).

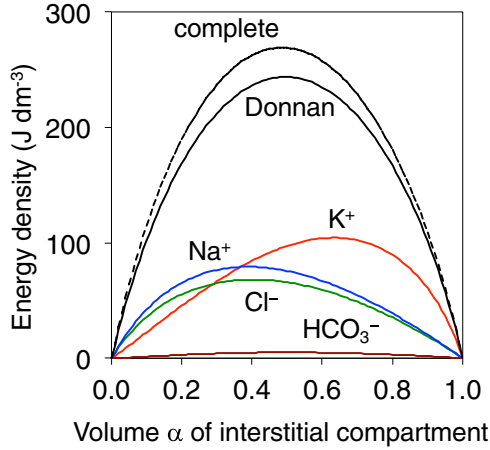


FIG. 5. Total work done by the four ion species of Table I when they mix, at constant volume, from their physiological concentrations to those at Donnan equilibrium (solid black curve labeled Donnan), and total work that would be done if they were able to mix completely (dotted black curve labeled complete). Colored curves plot, for each component ion species, the work of mixing to Donnan equilibrium.

As a theoretical point of reference, the black curve labeled complete in Fig. 5 plots the cumulative work that would be done if all four ion gradients mixed completely and independently to their equilibrium concentrations K_e calculated from Eq. (8). This curve has a greater peak energy of 269 J/l at $\alpha = 0.49$, but, as mentioned above, a complete mixing, being not electroneutral, would not be feasible.

B. Generation of the physiological ion gradients by the Na^+/K^+ pump

If the four ion gradients of Table I are ultimately to generate ATP by a reverse-mode operation of the Na^+/K^+ pump, then it must first be demonstrated that a normally operating pump is able to generate these gradients starting from the Donnan equilibrium. In particular, the concentrations must be shown to be consistent with the 3/2 stoichiometry of the pump.

The last column of Table I lists, for $\alpha = 0.2$, the number of ions transported from one compartment to the other during the mixing process, expressed as the number of charges per volume brain tissue in units of mol/m^3 or mM. Although the physiological gradient of K^+ is about three times greater than that of Na^+ , overall more Na^+ ions entered the cells during mixing than that K^+ ions left (24.7 versus 10.8 mM, similar ratios held at all values of α). These numbers can be reconciled with the 3/2 stoichiometry of the Na^+/K^+ pump if it is assumed that, during the buildup of the concentration gradients, part of the inward pumped K^+ ions left the cell again to expel Cl^- and HCO_3^- with them. Indeed, if the electrogenic component of the pumping (one-third of the transported Na^+ ions, the other two-thirds being balanced by K^+) is neutralized by the extrusion of Cl^- and HCO_3^- ions, then the outward pumped Na^+ ions can account for 8.2 mM of this anion transport. The remaining 5.7 mM of permeant anions need another channel for their extrusion, presumably the K^+/Cl^- cotransporter [13], using the K^+ gradient as energy. This implies that the total amount of inward pumped K^+ ions

during energy storage had been $10.8 + 5.7 = 16.5$ mM, or two-thirds of the amount of transported Na^+ ions, as required by the stoichiometry of the pump. This numerical relationship follows directly from the identity for electroneutrality:

$$\Delta\text{K}^+ + \Delta\text{Cl}^- + \Delta\text{HCO}_3^- = \Delta\text{Na}^+,$$

or

$$\Delta\text{K}^+ + (\Delta\text{Cl}^- + \Delta\text{HCO}_3^- - \frac{1}{3}\Delta\text{Na}^+) = \frac{2}{3}\Delta\text{Na}^+, \quad (30)$$

where the left-hand side of Eq. (30) indicates the total number of K^+ ions pumped inward during buildup of the gradients. The first term represents the K^+ ions that stay inside the cell (10.8 mM), the second term the K^+ ions that left the cell again together with Cl^- and HCO_3^- (5.7 mM). As explained above, the term between brackets can also be seen as the amount of anions that is expelled in excess of the electrogenic component of the Na^+/K^+ pump, and hence presumably is cotransported with K^+ .

In summary, this analysis, based on the electroneutrality of the Donnan equilibrium, justifies the assumption made in Sec. II that most of the electrical work done by the (electrogenic) Na^+/K^+ pump is converted into, and stored in, secondary gradients of other ions such as Cl^- and HCO_3^- .

C. Comparison of the energy stored in the ionic concentration gradients with that of the electrical membrane potential

To justify further the assumption that the buildup of the ion gradients, and by reciprocity also their breakdown during mixing, are electroneutral processes, the energy stored in the physiological ion gradients is next compared with that stored in the electrical potential difference across the neuron membrane separating the two compartments. The cerebellar granule cell is chosen for this comparison because its small size has enabled precise capacitance measurements to be made [40]. At a resting potential V_m of -65 mV, the cell membrane, which has a capacitance C_m of 3 pF [40], stores an energy $E = 0.5 C_m V_m^2 = 6.33$ fJ. Since at Donnan equilibrium V_m still measures -21 mV (Table I), the energy that can be retrieved from the membrane capacitor is further reduced to 2.91 fJ.

As for the energy stored in the ion gradients, given a specific membrane capacitance of $1 \mu\text{F}/\text{cm}^2$, the globular granule cell has the capacitance of a sphere of radius $4.9 \mu\text{m}$, with an intracellular volume of $V_2^* = \frac{4}{3}\pi r^3 = 4.93 \times 10^{-16} \text{ m}^3$. Taking again an extracellular volume fraction α of 0.2 [22,26], this implies that $V_1^* = 1.23 \times 10^{-16} \text{ m}^3$. These volumes and the concentrations of Table I were substituted into Eq. (6) to calculate the work done by the ions when they mix to their Donnan equilibrium at constant volume. For the Na^+ ions, the work done measured 39.9 pJ. For the K^+ , Cl^- , and HCO_3^- gradients, the respective values were 28.3, 34.1, and 1.69 pJ, giving a total work at $\alpha = 0.2$ of 104 pJ. Hence the energy stored in the granule cell's ion gradients is more than four orders of magnitude that stored in its electrical membrane potential, justifying the assumption of electroneutrality made in Sec. IV B [41,42].

Finally, from the molar number of transported Na^+ ions in Table I, it follows that 9.16×10^9 Na^+ ions would enter

TABLE II. Reported ion concentrations from ischemia experiments.

Ion species	Before ischemia (mM)		During ischemia (mM)	
	inside	outside	inside	outside
Na ⁺ ^a	10	154	35	59
K ⁺ ^a	134	3	106	60
Cl ⁻ ^b	11.4	128.3	32	89.2
A ⁻ ^c	134		134	
Total	289.4	285.3	307	208.2

^aSupplementary Table 1 of Ref. [44].

^bReference [43].

^cTable I

the granule cell during mixing. Given that the hydrolysis of one ATP molecule suffices to pump out 3 Na⁺ ions [11], the granule cell could, in theory, recover 3.05×10^9 molecules of ATP from a reversal of its Na⁺/K⁺ pump (at constant volume).

V. ESTIMATION OF THE ENERGY WHICH NEURONS CAN RETRIEVE FROM THEIR ION GRADIENTS DURING ISCHEMIA

An interruption of the energy supply to neurons, such as caused by reduced blood flow or ischemia, does not only break down the ion gradients but also induces neurons to swell and interstitial space to shrink [10,21,23–25,36]. Table II lists for the three major monovalent ion species the concentrations recorded during ischemia [43,44].

The analytical results of Secs. III D and III E (see also Appendixes D and E) are used here first to examine whether the reported concentration changes can be generated by ion and water transport in a two-compartmental model, and second to quantify the work done by mixing of the ions.

In general, changes in concentration can be a consequence of solute or solvent transport, or both (Fig. 1). The task is to find, for each given ion species and value of α , the ratio of solvent to solute transport that satisfies the initial and final concentrations (Table II) and conserves the number of particles [Eq. (2)]. In addition, to be consistent, the amount of transported solvent, and hence the resulting volume change, must be identical for all three ion species.

As explained in Sec. III D, the flows of solute and solvent are governed in the model by two parameters: parameter a specifies the ratio of solvent to solute transport [Eqs. (22) and (25)], whereas parameter w [Eq. (26)], by denoting the fractional change of the size of interstitial space (such that its final volume V_1° equals $w\alpha V$), quantifies solvent transport. For each ion species, the values of these parameters were calculated by substituting the initial and final concentrations of Table II, along with a given value of α , into Eqs. (25) and (26). The energy was then derived from Eq. (24), or its corollaries Eqs. (D18) and (E2). When no physical solution existed, for instance because the final volume V_1° was negative or greater than the total volume V , the energy was set to zero.

The left panels of Fig. 6 plot for each ion species (a) the work done by mixing and (b) the associated volume change w of interstitial space. It is clear, for instance, that only a limited

range of interstitial volumes α is compatible with the imposed changes in Na⁺ concentration (namely, those α at which the blue curve in (a) has a nonzero value). When α was too small (<0.18) the total amount of Na⁺ available in interstitial space would not suffice to raise the Na⁺ concentration in the cellular compartment [of size $(1 - \alpha)$] from 10 mM to the desired level of 35 mM during ischemia. In that case no physical solution existed. Beyond its peak, the work declines because, as α was increased, fewer Na⁺ ions needed to enter the smaller cellular compartment to cause the same rise in concentration. The energy profile is similar for Cl⁻ (black), but opposite

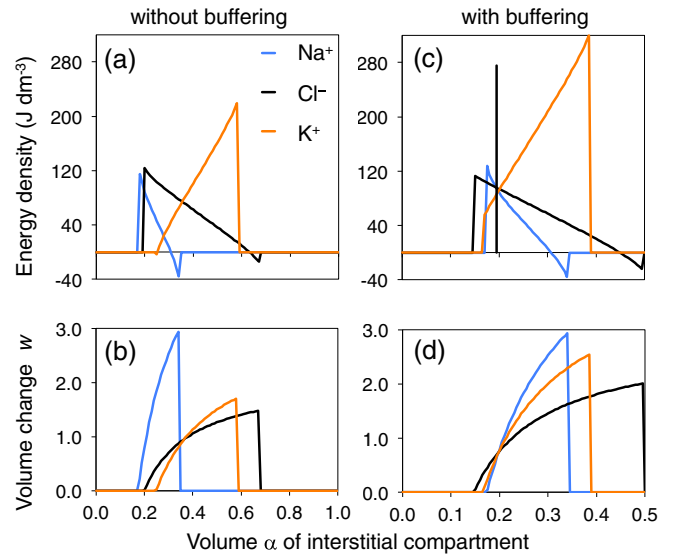


FIG. 6. Energy retrieved by mixing of the three major ion species during ischemia (Table II). The left column, (a) and (b), represents the plain model in the absence of buffering (Sec. III D). In the right column, (c) and (d), Cl⁻ and K⁺ ions were buffered in the interstitial compartment, using parameters $\gamma_{\text{Cl}} = 1.1$ and $\gamma_{\text{K}} = 1.2$ in Eq. (27) (Sec. III E and Appendix E). The bottom graphs, (b) and (d), plot the fractional change w of the volume of the interstitial compartment during the mixing of each ion species separately. The vertical black bar in (c) indicates the total energy density (276 J/l) at $\alpha = 0.195$, which is the size of the interstitial compartment at which mixing of each of the three ion species required an identical volume change in (d).

for K^+ (red), for which interstitial space constitutes the low-concentration compartment.

Although Fig. 6(a) shows that the concentration changes during ischemia (Table II) could be generated, for each ion species separately, by the combined transport of ions and water, no value of α was found at which the associated volume change w in (b) was identical for all three ion species. Making the final volumes coincide required the introduction of free parameters for the buffering of Cl^- and K^+ in interstitial space: $\gamma_{Cl} = 1.1$ and $\gamma_K = 1.2$ [see Eqs. (27)–(29)]. With these parameters added, the three volume profiles intersect at $\alpha = 0.195$ in Fig. 6(d), with a resulting shrinkage of interstitial space by 32% ($w = 0.68$). The total work at this intersection point measures 276 J/l [black bar in (c)]. To this work the mixing of Na^+ (34.1%), Cl^- (34.7%), and K^+ (31.2%) contributed almost equally. Note that this energy is 15.3% greater than that calculated from Eq. (7) for mixing at constant volume (using the same concentration changes and buffering parameters), but in that case the numbers of ions would not be conserved.

If the calculated energy of 276 J/l is compared with the ATP consumption rates mentioned in the literature (12–16 $\mu\text{mol/g/min} \approx 12\text{--}16$ J/l/s in [7], and 30 $\mu\text{mol/g/min} \approx 30$ J/l/s in [9] based on [45]), then the energy stored in the three major ion gradients would be able to substitute for ATP during 10–20 s. This is an upper limit because some buffering mechanisms presumed by the model, such as the uptake of interstitial K^+ by glial cells [39], may be ATP-dependent themselves, and because leak currents may dissipate part of the energy as heat [46].

VI. DISCUSSION

The present analytic treatment of the amount of energy that can be stored in concentration gradients is valid for any (charged or uncharged) compound, in both artificial and biological cells, but focuses on the ion gradients generated by the Na^+/K^+ pump across the cell membrane of neurons. In that case, the work done by mixing of the gradients can be conceived of as the production of ATP by a reversal of the pump [2–4, 11, 18, 19]. Two particular questions were addressed: the optimal path for energy retrieval (see Fig. 1) and the effect of the size of the interstitial (or extracellular) compartment.

The main result is that a concomitant contraction of the high-concentration compartment (paths C and D in Fig. 1) enhances the work of mixing, because the concentration gradient is maintained at a higher level throughout the mixing process (Sec. III C). The optimization of energy storage therefore amounts to finding the appropriate ratio of solvent to solute transport (Sec. III D and Fig. 3). The same principle, maintaining the concentration gradient, also underlies the optimal compartmental sizes for mixing at constant volume [Sec. III B and Eqs. (12) and (13)] and the increase of work in the presence of buffering (Sec. III E).

Mixing of multiple gradients, with changing compartmental volumes, was illustrated in Sec. V for the flow of Na^+ and Cl^- into the neurons during ischemia, accompanied by a swelling of the neurons and shrinkage of the interstitial compartment to an extent similar to that observed in experiments [24, 25, 36] (Fig. 6). The shrinkage of interstitial space and

swelling of the neurons must result from osmotic forces exerted by the impermeant intracellular anions that account for more than 40% of a neuron's osmolarity (A^- in Table I), and which, secondarily, enhance the osmotic imbalance during Donnan equilibration (Table I) and during ischemia (Table II).

The osmotic forces were not modeled explicitly in the present study, but water was assumed to follow passively the flow of solute through water-solute cotransporter channels. Actual neurons lack specific water channels in their cell membrane, and water is cotransported in a fixed stoichiometry with other substances such as KCl, using the solute gradients as energy [13, 37]. Hence the mechanism described in Sec. IV B for the expulsion of Cl^- out of the cells during the buildup of the ion gradients—via K^+/Cl^- cotransporters using the K^+ gradient generated by the Na^+/K^+ pump—will at the same time reduce the cellular volume and so lead to an expansion of interstitial space, as has been observed during sleep [26, 27]. Under conditions of ischemia or neuronal hyperactivity, the flow through cotransporter channels may reverse, so that water enters the cells via Cl^- cotransporters [36], causing in this case interstitial space to shrink. The present study therefore offers an alternative functional interpretation of the large movements of fluid between the intra- and extracellular compartment of the brain [26], namely, an optimization of energy storage.

The experimentally observed value of about 0.2 for α , the fraction of volume occupied by the interstitial compartment of the brain under physiological conditions [20–22, 26], is less straightforward to explain within the context of energy optimization. Although the optimal volume ratio for energy storage α_{opt} deviates considerably from 0.5 for single gradients [Eq. (11)], an asymmetry is needed to prevent the effects of inward and outward gradients from canceling each other (as they did in Fig. 5, where the total energy peaks at $\alpha = 0.5$). As shown in Sec. IV, neither the 3/2 stoichiometry of the Na^+/K^+ pump nor the intracellular abundance of impermeant anions (the Donnan effect) sufficed in this respect. The required asymmetry can be generated, instead, by the buffering of compound in one of the compartments (Sec. III E and Fig. 4). For instance, the experimentally observed concentration changes listed in Table II could only be reproduced if the K^+ and Cl^- ions were buffered in the interstitial compartment (Fig. 6). The effect of this buffering was to move the energy curves for K^+ and Cl^- towards smaller values of α [Fig. 6(c)], until, at a value of $\alpha = 0.195$, the water transport associated with the flows of K^+ and Cl^- coincided with that for (unbuffered) Na^+ [Fig. 6(d)].

The presumed physiological mechanism underlying this buffering is the uptake of interstitial K^+ ions by glial cells [25, 38, 39, 47]. In the present model, buffering of a compound is equivalent to a virtual enlargement of its compartment [Sec. III E and Eq. (28)], and it is noteworthy in this respect that the appearance of glial cells during growth and development coincides with a reduction of α from 0.4 to 0.2 [20, 21]. Nevertheless, it is difficult to determine the precise position of glial cells in a two-compartmental model [48]. Surely, glial cells have an active Na^+/K^+ pump and their K^+ gradient is similar to, or greater than, that of neurons [8, 12, 39]. On the other hand, they are able to clear the K^+ ions which neurons release into interstitial space, owing to a different kinetics

of their Na^+/K^+ pump [49] and the expression of inward rectifying ($K_{ir,4.1}$) K^+ channels [39,49]. In that respect, the glial cells would constitute a third compartment. In Sec. V this ambivalence was resolved by assigning them a buffering function in the interstitial compartment. Note further that the interstitial compartment of the brain communicates with the cerebrospinal fluid and the vascular compartment, so that its actual buffering capacity may be time dependent. To reduce such confounding effects, the ion concentrations in Table II were taken from ischemia experiments, in which the blood flow is reduced.

Finally, from the present study, there are two further reasons why having a small interstitial compartment ($\alpha = 0.2$) may be beneficial, apart from leaving more room for the vital intracellular substances, and providing Na^+ and Cl^- with a larger low-concentration compartment. First, it was shown in

Sec. III C that if there are (mechanical) limitations on the volume by which a compartment can shrink, then this limiting contraction volume may also constitute the optimal volume for energy storage (see red curve in Fig. 2). Such limitations on the swelling of neurons, and hence on the shrinkage of interstitial space, may be imposed by intracellular mechanical forces, or restrictions on the surface area of the cell membrane [50,51].

Second, a small volume fraction α for interstitial space may also minimize unwanted fluctuations of the physiological gradients of Na^+ and Cl^- and their Nernst potentials. As indicated in Sec. III B, there is an optimal volume ratio at which the flux of an ion least affects its gradient [Eq. (13)]. Using the physiological concentrations of Table I, the resulting values of α were 0.22 and 0.21 for Na^+ and Cl^- , the ions carrying most of the excitatory and inhibitory synaptic currents, respectively.

APPENDIX A: WORK OF MIXING AT CONSTANT VOLUME

During the mixing process, the compartments retain their initial volumes, hence $V_1^\circ = V_1^*$ and $V_2^\circ = V_2^*$. Starting from Eq. (5),

$$\begin{aligned}
 \left(\frac{\Delta G}{RT}\right)_{V_1} &= V_1^* \int_{K_1^\circ}^{K_1^*} \ln K_1 dK_1 - V_1^* \int_{K_2^\circ}^{K_2^*} \ln K_2 dK_2 \\
 &= V_1^* \int_{K_1^\circ}^{K_1^*} \ln K_1 dK_1 + V_2^* \int_{K_2^\circ}^{K_2^*} \ln K_2 dK_2 \\
 &= V_1^* [K_1 (\ln K_1 - 1)]_{K_1^\circ}^{K_1^*} + V_2^* [K_2 (\ln K_2 - 1)]_{K_2^\circ}^{K_2^*} \\
 &= V_1^* K_1^* \ln K_1^* - V_1^* K_1^\circ \ln K_1^\circ + V_1^* K_1^\circ - V_2^* K_2^* \ln K_2^* - V_2^* K_2^\circ \ln K_2^\circ + V_2^* K_2^\circ \\
 &= V_1^* K_1^* \ln K_1^* - V_1^* K_1^\circ \ln K_1^\circ + V_2^* K_2^* \ln K_2^* - V_2^* K_2^\circ \ln K_2^\circ.
 \end{aligned} \tag{A1}$$

The derivation of Eq. (12) goes as follows:

$$\begin{aligned}
 \lim_{\Delta K \rightarrow 0} \frac{1}{\Delta K} \left(\ln \frac{K_1}{K_2} - \ln \frac{K_1 - \frac{\Delta K}{V_1}}{K_2 + \frac{\Delta K}{V_2}} \right) &= \lim_{\Delta K \rightarrow 0} \frac{1}{\Delta K} \ln \frac{K_1}{K_2} \frac{K_2 + \frac{\Delta K}{V_2}}{K_1 - \frac{\Delta K}{V_1}} \\
 &= \lim_{\Delta K \rightarrow 0} \frac{1}{\Delta K} \ln \frac{1 + \frac{\Delta K}{V_2 K_2}}{1 - \frac{\Delta K}{V_1 K_1}} \\
 &= \lim_{\Delta K \rightarrow 0} \frac{1}{\Delta K} \ln \left(1 + \frac{\Delta K}{V_2 K_2} \right) - \lim_{\Delta K \rightarrow 0} \frac{1}{\Delta K} \ln \left(1 - \frac{\Delta K}{V_1 K_1} \right) \\
 &= \lim_{\Delta K \rightarrow 0} \frac{1}{V_2 K_2} \ln \left(1 + \frac{\Delta K}{V_2 K_2} \right)^{V_2 K_2 / \Delta K} + \lim_{\Delta K \rightarrow 0} \frac{1}{V_1 K_1} \ln \left(1 - \frac{\Delta K}{V_1 K_1} \right)^{-V_1 K_1 / \Delta K} \\
 &= \frac{1}{V_2 K_2} + \frac{1}{V_1 K_1} \\
 &= \frac{1}{\alpha V K_1} + \frac{1}{(1 - \alpha) V K_2}.
 \end{aligned}$$

APPENDIX B: WORK OF MIXING WITH THE CONCENTRATION KEPT CONSTANT IN ONE OF THE COMPARTMENTS

Without loss of generality, during the mixing process volume V_1 shrinks from V_1^* to zero while concentration K_1 remains constant at its initial value K_1^* .

Starting from Eq. (14), and using Eq. (2),

$$\begin{aligned}
 \left(\frac{\Delta G}{RT}\right)_{K_1} &= K_1^* \int_0^{V_1^*} \ln K_1^* dV_1 - K_1^* \int_0^{V_1^*} \ln K_2 dV_1 \\
 &= K_1^* \ln K_1^* \int_0^{V_1^*} dV_1 - K_1^* \int_0^{V_1^*} \ln \frac{K_{\text{tot}} - V_1 K_1^*}{V - V_1} dV_1
 \end{aligned}$$

$$\begin{aligned}
&= V_1^* K_1^* \ln K_1^* - K_1^* \int_0^{V_1^*} \ln(K_{\text{tot}} - V_1 K_1^*) dV_1 + K_1^* \int_0^{V_1^*} \ln(V - V_1) dV_1 \\
&= V_1^* K_1^* \ln K_1^* + \int_0^{V_1^*} \ln(K_{\text{tot}} - V_1 K_1^*) d(K_{\text{tot}} - V_1 K_1^*) - K_1^* \int_0^{V_1^*} \ln(V - V_1) d(V - V_1) \\
&= V_1^* K_1^* \ln K_1^* + \{(K_{\text{tot}} - V_1 K_1^*)[\ln(K_{\text{tot}} - V_1 K_1^*) - 1]\}_{V_1=0}^{V_1^*} - K_1^* [V_2(\ln V_2 - 1)]_{V_2}^{V_2^*} \\
&= V_1^* K_1^* \ln K_1^* + V_2^* K_2^* [\ln(V_2^* K_2^*) - 1] - K_{\text{tot}}(\ln K_{\text{tot}} - 1) - K_1^* V_2^* (\ln V_2^* - 1) + K_1^* V (\ln V - 1) \\
&= V_1^* K_1^* \ln K_1^* + V_2^* K_2^* \ln(V_2^* K_2^*) - K_{\text{tot}} \ln K_{\text{tot}} - K_1^* V_2^* \ln V_2^* + K_1^* V \ln V \\
&= V_1^* K_1^* \ln K_1^* + V_2^* K_2^* \ln K_2^* - K_{\text{tot}} \ln K_{\text{tot}} - (K_1^* - K_2^*) V_2^* \ln V_2^* + K_1^* V \ln V \\
&= V_1^* K_1^* \ln K_1^* + V_2^* K_2^* \ln K_2^* - K_{\text{tot}} \ln K_{\text{tot}} - (K_1^* - K_2^*) V_2^* \ln V_2^* + [K_{\text{tot}} + (K_1^* - K_2^*) V_2^*] \ln V \\
&= V_1^* K_1^* \ln K_1^* + V_2^* K_2^* \ln K_2^* - K_{\text{tot}} \ln \frac{K_{\text{tot}}}{V} - (K_1^* - K_2^*) V_2^* \ln \frac{V_2^*}{V}. \tag{B1}
\end{aligned}$$

APPENDIX C: EFFECT OF BUFFERING ON THE WORK OF MIXING AT CONSTANT CONCENTRATION

The derivation of Appendix B is repeated, but with compound K buffered in the second compartment. Following Eq. (27), the following substitution is used:

$$K_2 = \frac{K_{\text{tot}} - K_1 V_1}{V_2 + \gamma V_2^*} = \frac{K_{\text{tot}} - K_1 V_1}{V - V_1 + \gamma V_2^*},$$

$$\begin{aligned}
\left(\frac{\Delta G}{RT}\right)_{K_1, \text{buffer}} &= K_1^* \int_0^{V_1^*} \ln K_1^* dV_1 - K_1^* \int_0^{V_1^*} \ln K_2 dV_1 \\
&= K_1^* \ln K_1^* \int_0^{V_1^*} dV_1 - K_1^* \int_0^{V_1^*} \ln \frac{K_{\text{tot}} - V_1 K_1^*}{V - V_1 + \gamma V_2^*} dV_1 \\
&= V_1^* K_1^* \ln K_1^* - K_1^* \int_0^{V_1^*} \ln(K_{\text{tot}} - V_1 K_1^*) dV_1 + K_1^* \int_0^{V_1^*} \ln(V - V_1 + \gamma V_2^*) dV_1 \\
&= V_1^* K_1^* \ln K_1^* + \int_0^{V_1^*} \ln(K_{\text{tot}} - V_1 K_1^*) d(K_{\text{tot}} - V_1 K_1^*) \\
&\quad - K_1^* \int_0^{V_1^*} \ln(V - V_1 + \gamma V_2^*) d(V - V_1 + \gamma V_2^*) \\
&= V_1^* K_1^* \ln K_1^* + \{(K_{\text{tot}} - V_1 K_1^*)[\ln(K_{\text{tot}} - V_1 K_1^*) - 1]\}_{V_1=0}^{V_1^*} \\
&\quad - K_1^* \{(V_2 + \gamma V_2^*)[\ln(V_2 + \gamma V_2^*) - 1]\}_{V_2}^{V_2^*},
\end{aligned}$$

which further reduces to

$$\begin{aligned}
\left(\frac{\Delta G}{RT}\right)_{K_1, \text{buffer}} &= V_1^* K_1^* \ln K_1^* + (1 + \gamma) V_2^* K_2^* \ln K_2^* - K_{\text{tot}} \ln \frac{K_{\text{tot}}}{V_1^* + (1 + \gamma) V_2^*} \\
&\quad - (K_1^* - K_2^*) (1 + \gamma) V_2^* \ln \frac{(1 + \gamma) V_2^*}{V_1^* + (1 + \gamma) V_2^*},
\end{aligned}$$

where $K_{\text{tot}}/[V_1^* + (1 + \gamma) V_2^*]$ is the equilibrium concentration of K when K has spread over the entire volume, the first (nonbuffered) compartment having shrunk to zero.

Note that this result is also obtained directly from Eq. (B1), by substituting $(1 + \gamma) V_2^*$ for V_2^* and $V_1^* + (1 + \gamma) V_2^*$ for the total volume V .

APPENDIX D: WORK OF MIXING WITH BOTH CONCENTRATION AND VOLUME VARYING

Following Eqs. (3) and (22), take

$$\Delta V = a \Delta K,$$

where ΔV is an elementary volume of solvent that is transported in fixed proportion a to the element of solute ΔK . As noted in Sec. III D, if $aK_1^* = 1$ then the solute flows out of the compartment at a concentration identical to that of the compartment it leaves, hence $K_1^\circ = K_1^*$ (see path C in Fig. 1). This case was treated in Sec. III C and Appendix B.

In contrast, provided $aK_1^* \neq 1$, the development proceeds as follows:

$$\begin{aligned} dK &= d(K_1 V_1) \\ &= K_1 dV_1 + V_1 dK_1 \\ &= aK_1 dK + V_1 dK_1 \\ &= \frac{V_1 dK_1}{1 - aK_1}, \end{aligned} \quad (\text{D1})$$

and

$$dV_1 = adK = \frac{aV_1 dK_1}{1 - aK_1}. \quad (\text{D2})$$

Integration yields

$$V_1 = \frac{C}{1 - aK_1}, \quad (\text{D3})$$

where the integration constant C is given by

$$C = V_1^*(1 - aK_1^*), \quad (\text{D4})$$

so that, combining Eqs. (D1), (D2), and (D4),

$$dK = \frac{C}{(1 - aK_1)^2} dK_1. \quad (\text{D5})$$

In the same way, a constant D can be defined as

$$\begin{aligned} D &= V - C - aK_{\text{tot}} \\ &= V_1 + V_2 - V_1(1 - aK_1) - aV_1 K_1 - aV_2 K_2 \\ &= V_2(1 - aK_2) = V_2^*(1 - aK_2^*). \end{aligned} \quad (\text{D6})$$

Then, starting from Eq. (4), and using Eq. (D5),

$$\begin{aligned} \frac{\Delta G}{RT} &= \int_{K_1^\circ}^{K_1^*} \ln \frac{K_1}{K_2} dK \\ &= \int_{K_1^\circ}^{K_1^*} \frac{C}{(1 - aK_1)^2} \ln \frac{K_1}{K_2} dK_1 \\ &= \frac{C}{a} \int_{K_1^\circ}^{K_1^*} \ln \frac{K_1}{K_2} d \frac{1}{(1 - aK_1)} \\ &= \frac{C}{a} \int_{K_1^\circ}^{K_1^*} \ln K_1 d \frac{1}{(1 - aK_1)} - \frac{C}{a} \int_{K_1^\circ}^{K_1^*} \ln K_2 d \frac{1}{(1 - aK_1)}. \end{aligned} \quad (\text{D7})$$

The first integral of Eq. (D8) can be integrated by parts as

$$\begin{aligned} \frac{C}{a} \int_{K_1^\circ}^{K_1^*} \ln K_1 d \frac{1}{(1 - aK_1)} &= \frac{C}{a} \left[\frac{\ln K_1}{1 - aK_1} \right]_{K_1^\circ}^{K_1^*} - \frac{C}{a} \int_{K_1^\circ}^{K_1^*} \frac{1}{K_1(1 - aK_1)} dK_1 \\ &= \frac{C}{a} \left[\frac{\ln K_1}{1 - aK_1} \right]_{K_1^\circ}^{K_1^*} - \frac{C}{a} \int_{K_1^\circ}^{K_1^*} \frac{1}{K_1} dK_1 - \frac{C}{a} \int_{K_1^\circ}^{K_1^*} \frac{a}{1 - aK_1} dK_1 \\ &= \frac{C}{a} \left[\frac{\ln K_1}{1 - aK_1} - \ln K_1 \right]_{K_1^\circ}^{K_1^*} + \frac{C}{a} \int_{K_1^\circ}^{K_1^*} \frac{1}{\frac{1 - aK_1}{C}} d \left(\frac{1 - aK_1}{C} \right) \\ &= C \left[\frac{K_1 \ln K_1}{1 - aK_1} \right]_{K_1^\circ}^{K_1^*} + \frac{C}{a} \int_{V_1^\circ}^{V_1^*} V_1 d \frac{1}{V_1} \\ &= [V_1 K_1 \ln K_1]_{K_1^\circ}^{K_1^*} - \left[\frac{C}{a} \ln V_1 \right]_{V_1^\circ}^{V_1^*}. \end{aligned} \quad (\text{D9})$$

Provided $aK_2^* \neq 1$, and using D defined in Eq. (D6), the second integral of Eq. (D8) can be developed as

$$\begin{aligned} \frac{C}{a} \int_{K_1^\circ}^{K_1^*} \ln K_2 d \frac{1}{(1 - aK_1)} &= \frac{1}{a} \int_{V_1^\circ}^{V_1^*} \ln K_2 dV_1 \\ &= \frac{1}{a} \int_{K_2^\circ}^{K_2^*} \ln K_2 d \left(V - \frac{D}{1 - aK_2} \right) \\ &= -\frac{D}{a} \int_{K_2^\circ}^{K_2^*} \ln K_2 d \frac{1}{(1 - aK_2)}. \end{aligned}$$

Equation (D9) can then be used to solve this last integral, so that the full solution, Eq. (D8), reads

$$\frac{\Delta G}{RT} = [V_1 K_1 \ln K_1]_{K_1^\circ}^{K_1^*} + [V_2 K_2 \ln K_2]_{K_2^\circ}^{K_2^*} - \left[\frac{C}{a} \ln V_1 \right]_{V_1^\circ}^{V_1^*} - \left[\frac{D}{a} \ln V_2 \right]_{V_2^\circ}^{V_2^*}. \quad (\text{D10})$$

The notation of solution (D10) can be further simplified by introducing the coefficients w , x , y , and z , so as to write the final volumes and concentrations as $V_1^\circ = wV_1^*$, $K_1^\circ = xK_1^*$, $V_2^\circ = yV_2^*$, and $K_2^\circ = zK_2^*$. If w is given [or has been calculated from

Eq. (D20) below], then y is determined from the conservation of volume [Eq. (1)] by

$$y = \frac{V - wV_1^*}{V_2^*}. \quad (\text{D11})$$

To w and y , respectively, x and z are related by Eqs. (D4) and (D6)

$$C = V_1^\circ(1 - aK_1^\circ) = wV_1^*(1 - axK_1^*), \quad (\text{D12})$$

$$D = V_2^\circ(1 - aK_2^\circ) = yV_2^*(1 - azK_2^*), \quad (\text{D13})$$

from which

$$x = \frac{V_1^* - \frac{C}{w}}{V_1^* - C}, \quad (\text{D14})$$

$$z = \frac{V_2^* - \frac{D}{y}}{V_2^* - D}. \quad (\text{D15})$$

Using these four coefficients, Eq. (D10) simplifies to

$$\begin{aligned} \frac{\Delta G}{RT} &= [V_1 K_1 \ln K_1]_{xK_1^*}^{K_1^\circ} + [V_2 K_2 \ln K_2]_{zK_2^*}^{K_2^\circ} - \left[\frac{C}{a} \ln V_1 \right]_{wV_1^*}^{V_1^*} - \left[\frac{D}{a} \ln V_2 \right]_{yV_2^*}^{V_2^*} \\ &= V_1^* K_1^* \ln K_1^* - wxV_1^* K_1^* \ln(xK_1^*) + V_2^* K_2^* \ln K_2^* - yzV_2^* K_2^* \ln(zK_2^*) \\ &\quad + \frac{C}{a} \ln w + \frac{D}{a} \ln y \end{aligned} \quad (\text{D16})$$

or, using Eq. (1),

$$\begin{aligned} \frac{\Delta G}{RTV} &= \alpha K_1^* \ln K_1^* - wx\alpha K_1^* (\ln K_1^* + \ln x) + (1 - \alpha) K_2^* \ln K_2^* - yz(1 - \alpha) K_2^* (\ln K_2^* + \ln z) \\ &\quad + \frac{\alpha}{a} (1 - aK_1^*) \ln w + \frac{1 - \alpha}{a} (1 - aK_2^*) \ln y \end{aligned} \quad (\text{D17})$$

$$\begin{aligned} &= \alpha(1 - wx) K_1^* \ln K_1^* - wx\alpha K_1^* \ln x + (1 - yz)(1 - \alpha) K_2^* \ln K_2^* - yz(1 - \alpha) K_2^* \ln z \\ &\quad + \frac{\alpha}{a} (1 - aK_1^*) \ln w + \frac{1 - \alpha}{a} (1 - aK_2^*) \ln y. \end{aligned} \quad (\text{D18})$$

From this general expression [Eq. (D18)], the special solutions of Secs. III B and III C are derived as follows. Taking $w = y = 1$ yields the work done by mixing at constant volume [Eq. (7), corresponding to path A in Fig. 1]. Setting $a = 1/K_1^*$ and $x = 1$, and writing $\omega = w\alpha$, reduces Eq. (D18) to Eq. (20) (path C). Last, if there is only flow of solvent without solute transport (path B), then the concentration in each compartment changes in inverse proportion to volume, and the energy vanishes. This is seen by setting $wx = yz = 1$ and letting $a \rightarrow \infty$.

If, instead of a and w , the initial and final concentrations K_1^* , K_1° , K_2^* , and K_2° are given, then the values of a and w can be derived for each initial volume α . For instance, using Eqs. (D12) and (D13) to find expressions for w and y , and substituting these into Eq. (D11), yields

$$a = \frac{\alpha(K_1^* - K_1^\circ) + (1 - \alpha)(K_2^* - K_2^\circ)}{\alpha(K_1^* - K_1^\circ)K_2^\circ + (1 - \alpha)(K_2^* - K_2^\circ)K_1^\circ}, \quad (\text{D19})$$

and, using Eq. (D12),

$$w = (1 - aK_1^*) / (1 - aK_1^\circ). \quad (\text{D20})$$

APPENDIX E: EFFECT OF BUFFERING ON THE WORK OF MIXING WITH VARYING CONCENTRATION AND VOLUME

As in Appendix C, and without loss of generality, the buffer resides in the second compartment, and the first compartment contracts during the mixing process. Using Eq. (27), and applying the same substitutions as in Appendix C, the analysis of Appendix D can be modified as follows.

With constant D now reading

$$D = (1 + \gamma)V_2^*(1 - aK_2^*), \quad (\text{E1})$$

Eq. (D8) becomes

$$\frac{\Delta G}{RT} = [V_1 K_1 \ln K_1]_{K_1^\circ}^{K_1^*} + [(V_2 + \gamma V_2^*) K_2 \ln K_2]_{K_2^\circ}^{K_2^*} - \left[\frac{C}{a} \ln V_1 \right]_{V_1^\circ}^{V_1^*} - \left[\frac{D}{a} \ln(V_2 + \gamma V_2^*) \right]_{V_2^\circ + \gamma V_2^*}^{V_2^* + \gamma V_2^*}. \quad (\text{E2})$$

Note that the buffer capacity, or the size $V_b = \gamma V_2^*$ of the virtual extension of the buffering compartment [see Eq. (28)], is assumed to remain constant during shrinkage of the first, and expansion of the second, compartment. If, as before in Eq. (D11), y indicates the relative expansion of the second compartment excluding the buffer, then the whole second compartment measures $(y + \gamma)V_2^*$ after expansion, and its relative expansion is $(y + \gamma)/(1 + \gamma)$.

With the value of z in Eq. (D15) modified to

$$z = \frac{V_2^* - \frac{D}{y+\gamma}}{V_2^* - \frac{D}{1+\gamma}},$$

Eq. (D16) becomes

$$\begin{aligned} \frac{\Delta G}{RT} &= [V_1 K_1 \ln K_1]_{xK_1^\circ}^{K_1^*} + [(V_2 + \gamma V_2^*) K_2 \ln K_2]_{zK_2^\circ}^{K_2^*} - \left[\frac{C}{a} \ln V_1 \right]_{wV_1^\circ}^{V_1^*} - \left[\frac{D}{a} \ln(V_2 + \gamma V_2^*) \right]_{yV_2^* + \gamma V_2^*}^{V_2^* + \gamma V_2^*} \\ &= V_1^* K_1^* \ln K_1^* - wxV_1^* K_1^* \ln(xK_1^*) + (1 + \gamma)V_2^* K_2^* \ln K_2^* - (y + \gamma)zV_2^* K_2^* \ln(zK_2^*) \\ &\quad + \frac{C}{a} \ln w + \frac{D}{a} \ln \frac{y + \gamma}{1 + \gamma}. \end{aligned} \quad (\text{E3})$$

Finally, Eq. (D19) needs to be modified to

$$a = \frac{\alpha(K_1^* - K_1^\circ) + (1 + \gamma)(1 - \alpha)(K_2^* - K_2^\circ)}{\alpha(K_1^* - K_1^\circ)K_2^\circ + (1 + \gamma)(1 - \alpha)(K_2^* - K_2^\circ)K_1^\circ}. \quad (\text{E4})$$

-
- [1] W. van Egmond, M. Saakes, S. Porada, T. Meuwissen, C. Buisman, and H. Hamelers, The concentration gradient flow battery as electricity storage system: Technology potential and energy dissipation, *J. Power Sources* **325**, 129 (2016).
- [2] A. L. Lehninger, *Biochemistry* (Worth, New York, 1975).
- [3] P. Mitchell, David Keilin's respiratory chain concept and its chemiosmotic consequences, *Science* **206**, 1148 (1979).
- [4] D. G. Nicholls, *Bioenergetics* (Academic, London, 1982).
- [5] C. M. Armstrong, The Na/K pump, Cl ion, and osmotic stabilization of cells, *Proc. Natl. Acad. Sci. U.S.A.* **100**, 6257 (2003).
- [6] J. Astrup, P. M. Sørensen, and H. R. Sørensen, Oxygen and glucose consumption related to Na⁺-K⁺ transport in canine brain, *Stroke* **12**, 726 (1981).
- [7] M. Erecińska and I. A. Silver, ATP and brain function, *J. Cereb. Blood Flow Metab.* **9**, 2 (1989).
- [8] M. Erecińska and I. A. Silver, Ions and energy in mammalian brain, *Prog. Neurobiol.* **43**, 37 (1994).
- [9] D. Attwell and S. B. Laughlin, An energy budget for signaling in the grey matter of the brain, *J. Cereb. Blood Flow Metab.* **21**, 1133 (2001).
- [10] A. J. Hansen, Effect of anoxia on ion distribution in the brain, *Physiol. Rev.* **65**, 101 (1985).
- [11] I. M. Glynn, A hundred years of sodium pumping, *Annu. Rev. Physiol.* **64**, 1 (2002).
- [12] N. J. Gerkau, C. Rakers, G. C. Petzold, and C. R. Rose, Differential effects of energy deprivation on intracellular sodium homeostasis in neurons and astrocytes, *J. Neurosci. Res.* **95**, 2275 (2017).
- [13] E. Delpire and K. J. Staley, Novel determinants of the neuronal Cl⁻ concentration, *J. Physiol. (London)* **592**, 4099 (2014).
- [14] N. Zerangue and M. P. Kavanaugh, Flux coupling in a neuronal glutamate transporter, *Nature (London)* **383**, 634 (1996).
- [15] C. M. Armstrong, Packaging life: the origin of ion-selective channels, *Biophys. J.* **109**, 173 (2015).
- [16] C. Ayata and M. Lauritzen, Spreading depression, spreading depolarizations, and the cerebral vasculature, *Physiol. Rev.* **95**, 953 (2015).
- [17] O. Herreras and J. Makarova, Mechanisms of the negative potential associated with Leão's spreading depolarization: A history of brain electrogenesis, *J. Cereb. Blood Flow Metab.* **40**, 1934 (2020).
- [18] P. J. Garrahan and I. M. Glynn, The incorporation of inorganic phosphate into adenosine triphosphate by reversal of the sodium pump, *J. Physiol. (London)* **192**, 237 (1967).
- [19] P. De Weer and R. F. Rakowski, Current generated by backward-running electrogenic Na pump in squid giant axons, *Nature (London)* **309**, 450 (1984).
- [20] A. Lehmenkühler, E. Syková, J. Svoboda, K. Zilles, and C. Nicholson, Extracellular space parameters in the rat neocortex and subcortical white matter during postnatal development determined by diffusion analysis, *Neuroscience* **55**, 339 (1993).
- [21] I. Voříšek and E. Syková, Ischemia-induced changes in the extracellular space diffusion parameters, K⁺, and pH in the developing rat cortex and corpus callosum, *J. Cereb. Blood Flow Metab.* **17**, 191 (1997).
- [22] C. Nicholson and S. Hrabětová, Brain extracellular space: The final frontier of neuroscience, *Biophys. J.* **113**, 2133 (2017).
- [23] P. W. Dierkes, H. J. Wüsten, G. Klees, A. Müller, and P. Hochstrate, Ionic mechanism of ouabain-induced swelling of

- leech Retzius neurons, *Pflugers Arch - Eur. J. Physiol* **452**, 25 (2006).
- [24] I. Dietzel and U. Heinemann, Dynamic variations of the brain cell microenvironment in relation to neuronal hyperactivity, *Ann. N.Y. Acad. Sci.* **481**, 72 (1986).
- [25] I. Dietzel, U. Heinemann, and H. D. Lux, Relations between slow extracellular potential changes, glial potassium buffering, and electrolyte and cellular volume changes during neuronal hyperactivity in cat brain, *Glia* **2**, 25 (1989).
- [26] L. Xie, H. Kang, Q. Xu, M. J. Chen, Y. Liao, M. Thiyagarajan, J. O'Donnell, D. J. Christensen, C. Nicholson, J. J. Iliff, T. Takano, R. Deane, and M. Nedergaard, Sleep drives metabolite clearance from the adult brain, *Science* **342**, 373 (2013).
- [27] R. Rasmussen, J. O'Donnell, F. Ding, and M. Nedergaard, Interstitial ions: A key regulator of state-dependent neural activity? *Prog. Neurobiol.* **193**, 101802 (2020).
- [28] J. Jäckle, The causal theory of the resting potential of cells, *J. Theor. Biol.* **249**, 445 (2007).
- [29] K. Dijkstra, J. Hofmeijer, S. A. van Gils, and M. J. van Putten, A biophysical model for cytotoxic cell swelling, *J. Neurosci.* **36**, 11881 (2016).
- [30] A. V. Dmitriev, A. A. Dmitriev, and R. A. Linsenmeier, The logic of ionic homeostasis: Cations are for voltage, but not for volume, *PLoS Comput. Biol.* **15**, e1006894 (2019).
- [31] J. N. Brønsted, *Physical Chemistry* (Heinemann, London, 1937).
- [32] K. Denbigh, *The Principles of Chemical Equilibrium*, 4th ed. (Cambridge University Press, Cambridge, UK, 1981).
- [33] G. B. Benedek and F. M. H. Villars, *Physics with Illustrative Examples from Medicine and Biology* (Springer-Verlag, New York, 2000).
- [34] J. Pods, A comparison of computational models for the extracellular potential of neurons, *J. Integr. Neurosci.* **16**, 19 (2017).
- [35] W. J. van Egmond, Concentration gradient flow batteries: salinity gradient energy systems as environmentally benign large scale electricity storage, Ph.D. thesis, Wageningen University, Wageningen, The Netherlands, 2018.
- [36] R. L. Rungta, H. B. Choi, J. R. Tyson, A. Malik, L. Dissing-Olesen, P. J. C. Lin, S. M. Cain, P. R. Cullis, T. P. Snutch, and B. A. MacVicar, The cellular mechanisms of neuronal swelling underlying cytotoxic edema, *Cell* **161**, 610 (2015).
- [37] N. MacAulay, S. Hamann, and T. Zeuthen, Water transport in the brain: Role of cotransporters, *Neuroscience* **129**, 1031 (2004).
- [38] A. R. Gardner-Medwin, Analysis of potassium dynamics in mammalian brain tissue, *J. Physiol. (London)* **335**, 393 (1983).
- [39] G. G. Somjen, H. Kager, and W. J. Wadman, Computer simulations of neuron-glia interactions mediated by ion flux, *J. Comput. Neurosci.* **25**, 349 (2008).
- [40] E. D'Angelo, G. De Filippi, P. Rossi, and V. Taglietti, Synaptic excitation of individual rat cerebellar granule cells in situ: evidence for the role of NMDA receptors, *J. Physiol. (London)* **484**, 397 (1995).
- [41] R. Maex, On the Nernst-Planck equation, *J. Integr. Neurosci.* **16**, 73 (2017).
- [42] S. L. Gratiy, K. H. Pettersen, G. T. Einevoll, and A. M. Dale, Pitfalls in the interpretation of multielectrode data: On the infeasibility of the neuronal current-source monopoles, *J. Neurophysiol.* **109**, 1681 (2013).
- [43] C. Jiang, S. Agulian, and G. G. Haddad, Cl^- and Na^+ homeostasis during anoxia in rat hypoglossal neurons: Intracellular and extracellular in vitro studies, *J. Physiol. (London)* **448**, 697 (1992).
- [44] J. P. Dreier, T. Isele, C. Reiffurth, N. Offenhauser, S. A. Kirov, M. A. Dahlem, and O. Herreras, Is spreading depolarization characterized by an abrupt, massive release of Gibbs free energy from the human brain cortex? *Neuroscientist* **19**, 25 (2013).
- [45] O. H. Lowry, J. V. Passonneau, F. X. Hasselberger, and D. W. Schulz, Effect of ischemia on known substrates and cofactors of the glycolytic pathway in brain, *J. Biol. Chem.* **239**, 18 (1964).
- [46] R. J. Clarke, M. Catauro, H. H. Rasmussen, and H. J. Apell, Quantitative calculation of the role of the Na^+, K^+ -ATPase in thermogenesis, *Biochim. Biophys. Acta* **1827**, 1205 (2013).
- [47] G. G. Somjen, Extracellular potassium in the mammalian central nervous system, *Annu. Rev. Physiol.* **41**, 159 (1979).
- [48] R. Jolivet, P. J. Magistretti, and B. Weber, Deciphering neuron-glia compartmentalization in cortical energy metabolism, *Front. Neuroenergetics* **1**, 4 (2009).
- [49] B. R. Larsen, A. Stoica, and N. MacAulay, Managing brain extracellular K^+ during neuronal activity: The physiological role of the Na^+/K^+ -ATPase subunit isoforms, *Front. Physiol.* **7**, 141 (2016).
- [50] F. Sachs and M. V. Sivaselvan, Cell volume control in three dimensions: Water movement without solute movement, *J. Gen. Physiol.* **145**, 373 (2015).
- [51] J. Tao and S. X. Sun, Active biochemical regulation of cell volume and a simple model of cell tension response, *Biophys. J.* **109**, 1541 (2015).